Behavioral/Cognitive

Dynamic Network Activation of Hypothalamic MCH Neurons in REM Sleep and Exploratory Behavior

Carlos Blanco-Centurion,[1] SiWei Luo,[1] Daniel J. Spergel,[2] Aurelio Vidal-Ortiz,[3] Sorinel A. Oprisan,[4] Anthony N. Van den Pol,[2] Meng Liu,[1] and Priyattam J. Shiromani[1,3]

[1]Departments of Psychiatry & Behavioral Sciences, Medical University of South Carolina, Charleston, South Carolina 29425, [2]Department of Neurosurgery, Yale University School of Medicine, New Haven, Connecticut 06520, [3]Laboratory of Sleep Neuroscience, Ralph H. Johnson VA Medical Center, Charleston, South Carolina 29401, and [4]Department of Physics and Astronomy, College of Charleston, Charleston, South Carolina 29424

Most brain neurons are active in waking, but hypothalamic neurons that synthesize the neuropeptide melanin-concentrating hormone (MCH) are claimed to be active only during sleep, particularly rapid eye movement (REM) sleep. Here we use deep-brain imaging to identify changes in fluorescence of the genetically encoded calcium (Ca^{2+}) indicator GCaMP6 in individual hypothalamic neurons that contain MCH. An *in vitro* electrophysiology study determined a strong relationship between depolarization and Ca^{2+} fluorescence in MCH neurons. In 10 freely behaving MCH-cre mice (male and female), the highest fluorescence occurred in all recorded neurons ($n = 106$) in REM sleep relative to quiet waking or non-REM sleep. Unexpectedly, 70% of the MCH neurons had strong fluorescence activity when the mice explored novel objects. Spatial and temporal mapping of the change in fluorescence between pairs of MCH neurons revealed dynamic activation of MCH neurons during REM sleep and activation of a subset of the same neurons during exploratory behavior. Functional network activity maps will facilitate comparisons of not only single-neuron activity, but also network responses in different conditions and disease.

Key words: **calcium imaging; hypothalamus; melanin concentrating hormone; REM sleep; sleep**

Significance Statement

Functional activity maps identify brain circuits responding to specific behaviors, including rapid eye movement sleep (REM sleep), a sleep phase when the brain is as active as in waking. To provide the first activity map of individual neurons during REM sleep, we use deep-brain calcium imaging in unrestrained mice to map the activity of hypothalamic melanin-concentrating hormone (MCH) neurons. MCH neurons were found to be synchronously active during REM sleep, and also during the exploration of novel objects. Spatial mapping revealed dynamic network activation during REM sleep and activation of a subset of the neurons during exploratory behavior. Functional activity maps at the cellular level in specific behaviors, including sleep, are needed to establish a brain connectome.

Introduction

An important goal in neuroscience is to map the circuits in the brain that are activated in response to specific behaviors. In humans, functional connectivity maps derived from functional MRI studies identify specific brain regions that are activated during rapid eye movement sleep (REM sleep; Chow et al., 2013), a period of sleep when the brain is as active as in waking. During waking specific circuits are required to accomplish the task, and activity in the circuit represents use-dependent function of the circuit (Picchioni et al., 2013). However, in REM sleep there is no sensory input, and still circuits are activated. The purpose of the activation during REM sleep is not known, but may be indicative

Received Feb. 6, 2019; revised March 8, 2019; accepted April 6, 2019.

Author contributions: A.N.V.d.P. and P.S. designed research; C.B.-C., S.L., D.J.S., A.V.-O., A.N.V.d.P., and P.J.S. performed research; M.L. and P.S. contributed unpublished reagents/analytic tools; C.B.-C., S.L., D.J.S., S.A.O., A.N.V.d.P., and P.S. analyzed data; C.B.-C. and P.S. wrote the paper.

This research was supported by National Institutes of Health Grants NS-052287, NS-079940, NS-098541, NS-096151, and NS-101469 (to M.L.), and DK-115933 and DK-084052 (to A.N.V.d.P.); and by the Medical Research Service of the Department of Veterans Affairs (Grant BX000798). P.S. is the recipient of a Senior Research Career Scientist Award (1K6BX004216) from the Department of Veterans Affairs. The contents of this work do not represent the views of the U.S. Department of Veterans Affairs or the United States Government. We thank laboratory members Dr. RodaRani Konadhode, Dr. Dheeraj Pelluru, Dr. Ying Sun, Bingyu Zou, and Emmaline Bendell for technical assistance. We also thank Dr. Shanna Resendiz at Inscopix for advice, guidance, and technical support regarding calcium imaging. In addition, we thank Dr. Paul J. Nietert, Medical University of South Carolina, for guidance on mixed models in SPSS.

The authors declare no competing financial interests.

Correspondence should be addressed to Priyattam J. Shiromani at shiroman@musc.edu or Meng Liu at liumen@musc.edu.

https://doi.org/10.1523/JNEUROSCI.0305-19.2019

of an internally cued cognitive state that underlies dreaming and memory consolidation (Nir and Tononi, 2010).

REM sleep is present in all mammals and birds, and may even extend to reptiles (Shein-Idelson et al., 2016). Functional connectivity maps have identified activation of specific regions in REM sleep in humans, but to establish a connectome of sleep it is necessary to identify activation of individual neuronal phenotypes during REM sleep. Some neuronal phenotypes, such as those containing norepinephrine (Aston-Jones and Bloom, 1981), serotonin (Wu et al., 2004), histamine (John et al., 2004) or orexin/hypocretin (Lee et al., 2005; Mileykovskiy et al., 2005) are considered to be arousal neurons because they are silent in REM sleep. Therefore, we focused on the hypothalamic neurons containing the neuropeptide melanin-concentrating hormone (MCH), which are intermingled with the arousal orexin and histamine neurons; MCH neurons are considered to be active only in sleep, particularly REM sleep (Hassani et al., 2009). MCH is a cyclic neuropeptide present in the hypothalamus of all vertebrates, and MCH neurons project widely throughout the brain (Nahon et al., 1989; Bittencourt et al., 1992; Elias et al., 1998; Peyron et al., 1998; Cvetkovic et al., 2004). Optogenetic stimulation of the MCH neurons induces sleep in both mice and rats (Jego et al., 2013; Konadhode et al., 2013; Tsunematsu et al., 2014; Blanco-Centurion et al., 2016), indicating a common neuronal phenotype driving sleep in at least rodents. The activity of MCH neurons in mice, where indices of REM sleep have been firmly validated, can be used to identify the activation of a common circuit in REM sleep.

In the present study, we use deep-brain imaging (Ghosh et al., 2011; Hamel et al., 2015) to measure Ca^{2+} gradients associated with enhanced neuronal activity (Tian et al., 2009) in individual neurons. The genetically encoded Ca^{2+} indicator (GCaMP) introduced into phenotype-specific neurons provides an index of depolarization of the neuron and serves as a readout of activity of the neuron (Chen et al., 2013). We discovered that in MCH-cre mice the MCH neurons show synchronized network activation during REM sleep. Unexpectedly, the MCH neurons were also activated during exploratory behavior, but not during walking, eating, or grooming. Spatial mapping of the relationship of the fluorescence between pairs of MCH neurons identified a dynamic pattern of network activation during REM sleep and the activity of subsets of the neurons during exploration of novel objects. Mapping activity patterns within a single neuronal phenotype provides a framework for the comparison of activity of the underlying network during different conditions and disease.

Materials and Methods

Approvals. All procedures in the mice were approved by institutional committees and abided by the National Institutes of Health protocols on the care and use of animals. The *in vitro* studies were approved by The Yale University Animal Use Committee, while the Ralph H. Johnson VA Institutional Animal Care and Use Committee approved all procedures for the *in vivo* studies in freely behaving mice (protocols 602 and 607).

Simultaneous Ca^{2+} imaging and whole-cell recording of MCH neurons in brain slices. For experiments involving simultaneous Ca^{2+} imaging and whole-cell recording, Cre-dependent expression of GCaMP6s in MCH neurons was obtained by injecting AAV1.CAG.FLEX.GCaMP6s.WPRE.SV40 (Chen et al., 2013; 3.208×10^{13} IU/ml titer; Penn Vector Core, Philadelphia, PA) bilaterally (1.5 μl each side) into the hypothalamus (−1.6 mm anteroposterior; ±1.25 mm mediolateral; −5.25 mm dorsoventral relative to bregma) of 1-month-old male MCH-Cre mice (Kong et al., 2010; The Jackson Laboratory; RRID:IMSR_JAX:014099). Three to 4 weeks later, 300-μm-thick coronal brain slices were prepared and GCaMP6s-expressing MCH neurons in the hypothalamus were imaged using a CCD camera (ORCA-ER, Hamamatsu) connected to an upright fluorescence microscope (BX51WI, Olympus), with a neutral density filter in the excitation light path to reduce light transmittance to 25% to minimize photobleaching. Images were acquired at 1 Hz, with an exposure time of 1 s, controlled by μManager software (Open Imaging), and analyzed for fluorescence changes using ImageJ software (National Institutes of Health, Bethesda, MD) and Igor Pro software (WaveMetrics). Whole-cell recordings, acquired with an EPC 9 patch-clamp amplifier (HEKA Elektronik), were obtained from the GCaMP6s-expressing MCH neurons immediately before Ca^{2+} imaging. The bath solution contained the following (in mM): 124 NaCl, 3 KCl, 2 $MgCl_2$, 2 $CaCl_2$, 1.23 NaH_2PO_4, 26 $NaHCO_3$, and 10 glucose (gassed with 95% O_2/5% CO_2; 300–305 mosmol/L). The pipette solution contained the following (in mM): 145 potassium gluconate, 1 $MgCl_2$, 10 HEPES, 1.1 EGTA, 2 Mg-ATP, 0.5 Na_2-GTP, and 5 Na_2-phosphocreatine, pH adjusted to 7.3 with KOH; 285–295 mosmol/L). Pipette and cell capacitance were compensated using PatchMaster software (HEKA Elektronik), which was also used to acquire and, together with Igor Pro software, analyze the data. Electrophysiological data were acquired at 10 kHz, filtered at 3 kHz, and corrected for the liquid junction potential, which was 8 mV.

In vivo *animals and surgery.* The MCH-Cre mice [hemizygous for Tg (PMCH-Cre)1Lowl; The Jackson Laboratory; RRID:IMSR_JAX:014099] were bred in our facilities and those that were Cre+, based on genotyping of tail snips (Transnetyx), were used. After surgery, the animals were housed singly in Plexiglas cages with bedding, and food and water were available *ad libitum*. The temperature in the sleep recording room was 25°C and a 12 h light/dark cycle (lights on 6:00 A.M. to 6:00 P.M.; 100 lux) was maintained. The mice were 171.4 d old (±27.72) and weighed 36.04 g (±3.81) at the time of surgery.

The mice were anesthetized (2% isoflurane), and, using a stereotaxic apparatus, the genetically encoded Ca^{2+} indicator GCaMP6s (AAV-DJ EF1a-DIO-GCaMP6s; 2–4 μl; $0.4 \times e^9/\mu$l infectious titer; stock #091, Stanford Gene Viral Vector Core) was injected slowly over a 10 min period into the lateral hypothalamus (relative to bregma A = −1.6 mm; lateral = 0.7 mm; ventral from brain surface = 4.8 mm). In three mice, GCaMP6m (1 μl; infectious titer, $12.8 \times e^9/\mu$l; stock #092, Stanford Gene Viral Vector Core) was injected as our supply of GCaMP6s stock was finished.

The viral injection cannula was held in place for 45 min and then slowly retracted. After delivery of the virus, a GRIN (graded index) lens (0.6 mm in diameter; 7.3 mm in length; stock #1050-002208, Inscopix) was inserted into the same cannula track and cemented to the skull. At this time, four screw electrodes for measuring the EEG were secured to the skull and two flexible wires were inserted into the nuchal muscles to measure the EMG. The electrodes and lens were secured to the skull with dental cement. The mice were administered carprofen for pain management. Ten days later, the mice were anesthetized (2% isoflurane) and placed in the stereotaxic instrument, and a single photon miniaturized fluorescence microscope [nVista miniature microscope (miniscope), Inscopix] with a baseplate was positioned atop the implanted GRIN lens. The baseplate of the microscope was secured to the lens with dental cement and the microscope was detached.

Time line of studies in freely behaving mice. Fourteen days after insertion of the Ca^{2+} indicator and lens, the mice were gently restrained (swaddled in terry cloth), a lightweight cable was attached to the EEG-EMG electrodes, and the miniature microscope was attached to the baseplate. The mice were returned to their home cage and allowed to adapt to the EEG tether and the microscope for 6–8 h periods in the day cycle (lights on) for 3 successive days. At the end of each adaptation period, the microscope was detached, a protective cover plate was attached to the baseplate, and the mice were returned to the vivarium.

The 3 d of adaption composed of adapting each animal to the miniscope, recording clear EEG-EMG signals, and identifying the focal plane of the miniscope that yielded the clearest fluorescence signal. In each animal, we began by making brief (1–5 min) morning recordings to identify the clarity of the fluorescence in neurons. We quickly learned that in the MCH neurons abundant and clear fluorescence occurred during REM sleep. Therefore, during these brief imaging sessions the

miniscope was switched on for 1–5 min once it was evident that the mouse was transitioning into REM sleep. The brief recording periods made it possible to quickly analyze (Mosaic software, Inscopix) the data, and if the fluorescence signal was not clear, then the miniscope was rotated by a quarter turn (25 μm; the full exertion of the miniscope is 300 μm). After establishing a focal plane that provided the sharpest fluorescence signal in neurons, we noted the position of the miniscope.

On the fourth day, at 9:00 A.M. (3 h after the start of the light cycle) the animals were instrumented as in the adaptation period and allowed to sleep undisturbed for 4–6 h. Ca^{2+} influx during natural sleep was recorded primarily in the second half of the lights-on period (2:00 to 6:00 P.M.) as the first half of the day cycle was reserved for adapting the mice to the miniscope. Ca^{2+} signals and sleep were recorded while the mice remained in their familiar home cages. Food and water were available *ad libitum* in the cage. The EEG, EMG, video of animal behavior, and Ca^{2+} influx were recorded for 1 h with complete cycles of wake, non-REM (NREM), and REM sleep.

Immediately after acquiring the data during natural sleep, the Ca^{2+} signal was monitored during a 10 min period of exploring novel objects.

Exploration of novel objects. In this test, the neurons were imaged during a 10 min period while the mice were exploring novel objects (e.g., binder clip, small plastic building block, bottle cap) placed in their home cage. The EEG, EMG, and behavior were recorded.

Ca^{2+} imaging in freely behaving mice. We imaged only at the focal plane that provided the sharpest depiction of the neurons. Ca^{2+} imaging data were recorded with nVista software (Inscopix) at 10 frames/second (fps) and 10% illumination setting (0.1 mW at the tip). The EEG and EMG signals were amplified via Grass amplifiers and recorded as analog signals on a Plexon Omniplex system. This system also recorded the behavior of the animal via a video camera synchronized with the EEG-EMG data. All data were analyzed off-line using specific software (Neuroexplorer, Nex Technologies; Inscopix; Plexon).

Calcium data were processed using Mosaic 1.2.0 (Inscopix). The GCaMP data were analyzed in an independent and blind manner. The initial nVista files were spatially reduced by a factor of two. We implemented preprocessing features to correct for defective pixilation, row noise, and dropped frames. Moreover, we corrected for motion artifacts to generate the steadiest calcium signal (<0.1 μm along the *x*–*y*-axis). The corrected movies were subsequently filtered (mean filter). Next, the average fluorescence of all the frames in the recording period was determined and represented in a single reference frame (F_0). Thus, F_0 represented the average fluorescence regardless of the sleep–wake state or wake behavior. The change in fluorescence ($\Delta F/F_0$) in each frame of the movie at a given time ($F(t)$) was determined against the single reference frame according to the following formula: $\Delta F/F_0 = ((F(t) - F_0)/F_0)$. Individual neurons [regions of interest (ROIs)] were automatically extracted from the normalized movie by the Mosaic software with principal component analysis (PCA) and independent component analysis (ICA). Each ROI (neuron) was identified as a neuron based on cell morphology. Output from the ICA consisted of both the maximum projection image for each neuron and its fluorescence trace were transformed to ($\Delta F/F_0$) versus time. The $\Delta F/F_0$ in each neuron was exported into Excel, whereas images were used for neuronal identification and mapping. In each mouse, the $\Delta F/F_0$ was expressed as a *z*-score. Thus, in each mouse the entire fluorescence dataset was standardized to *z*-scores regardless of sleep–wake behavior.

Recording of sleep and other behaviors. The sleep–wake states were identified based on EEG, EMG and video data (Neuroexplorer; Plexon). Active waking was identified by behavioral activity of the mice in the video, the presence of desynchronized EEG, and high EMG activity when the animals were walking, rearing, eating, grooming, or digging. Not all mice

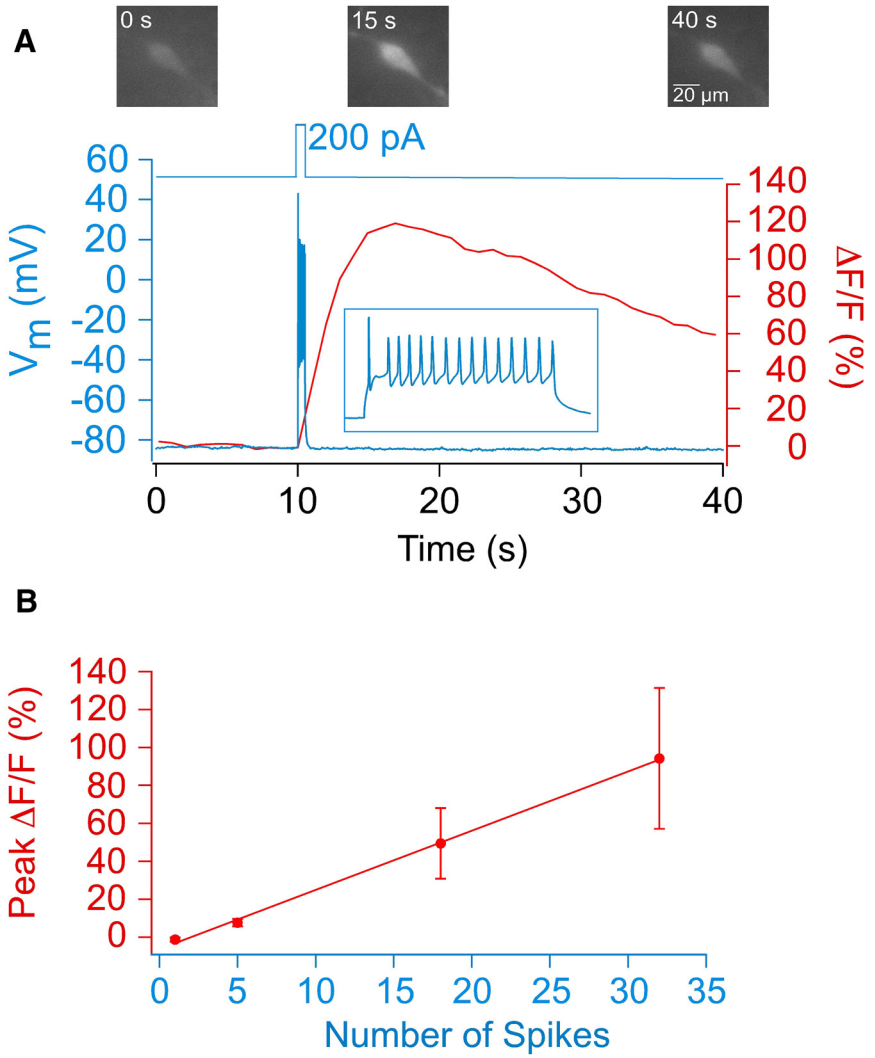

Figure 1. *In vitro* slice electrophysiology determines that GCaMP6s fluorescence is linearly related to the number of action potentials. ***A***, An *In vitro* slice electrophysiology experiment confirmed that increased GCaMP6 fluorescence ($\Delta F/F$), indicative of increased Ca^{2+}, was associated with depolarization and subsequent spike activity in GCaMP6s-expressing MCH neurons. Red trace shows increased GCaMP6 fluorescence (middle and right images, acquired at 15 and 40 s, respectively, vs left image, acquired at 0 s) following a spike train (blue trace) evoked by a 0.5 s injection (via the patch pipette) of depolarizing current (200 pA) in a GCaMP6s-expressing MCH neuron recorded in the whole-cell configuration in an MCH-Cre mouse brain slice. Individual spikes within the spike train are shown at higher temporal resolution in the boxed inset. In six MCH neurons (from four mice) imaged and recorded simultaneously, $\Delta F/F$ increased by 49.5 ± 18.7% (mean ± SEM) following a 0.5 s injection of 283 ± 124 pA of current that evoked a depolarization of 30.5 ± 4.5 mV from a resting membrane potential of −74.2 ± 4.7 mV and resulted in 18 ± 6 spikes (range, 2–37 spikes) with an amplitude (first spike) of 73.4 ± 7.3 mV. $\Delta F/F$ (%), fluorescence at time *t* ($F(t)$) − baseline fluorescence (F, averaged fluorescence in the 10 s period before current injection), divided by F and multiplied by 100, after the subtraction of background fluorescence (fluorescence from a cell-free region); V_m, membrane potential. ***B***, The plot shows the peak change in GCaMP6 fluorescence as a function of the number of spikes. Data points (left to right) are the mean ± SEM. values of peak $\Delta F/F$ (%) obtained from six MCH neurons (from four mice) following 10 ms, 100 ms, 0.5 s, and 1 s injections of depolarizing current that evoked 1 ± 0, 5 ± 1, 18 ± 6, and 32 ± 12 spikes, respectively.

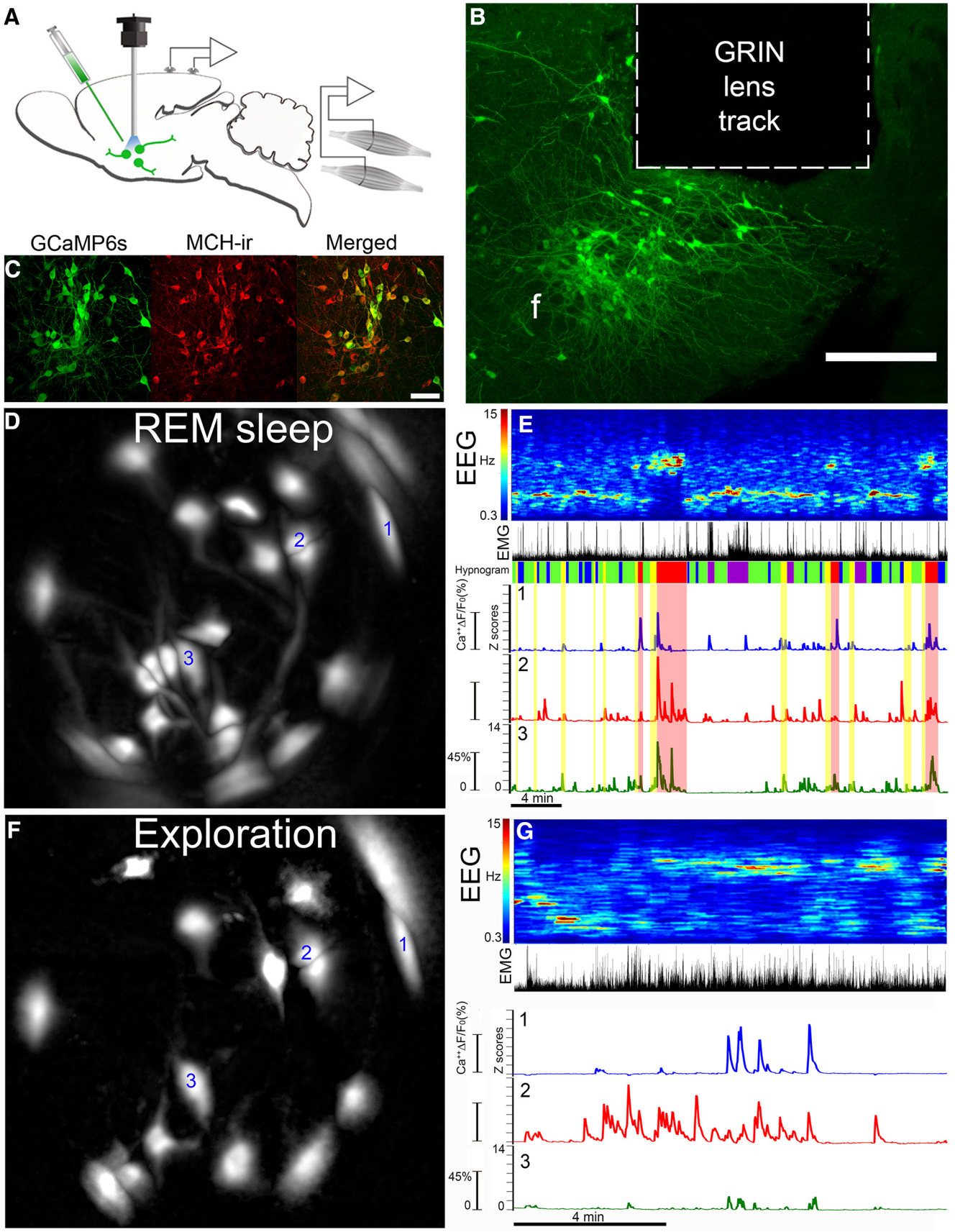

Figure 2. Deep-brain imaging of MCH neurons. ***A***, Schematic of transfection of MCH neurons in MCH-Cre mice with AAV-DIO-GCaMP6 followed by placement of the GRIN lens in region transfected with GCaMP6 (slow or medium). The miniscope is attached to the GRIN lens via a baseplate on the skull. ***B***, Photomicrograph depicts the location of the GRIN lens (outlined in dashed lines) atop the body of GCaMP6s containing neurons in the hypothalamus in a representative MCH-Cre mouse. The brain region containing the GRIN lens was sectioned along the coronal axis of the brain, and tissue containing the GCaMP6s neurons were identified. f, Fornix. Scale bar, 300 μm. ***C***, Immunohistochemistry revealed that GCaMP6s-infected neurons (green) were also (*Figure legend continues.*)

engaged in all of these behaviors. Quiet waking was identified by desynchronized EEG, lower EMG tone relative to active waking, and lack of behavioral activity in the video. NREM sleep consisted of high-amplitude slow waves together with a low EMG tone relative to waking and sleeping posture on the video. Pre-REM sleep (REM transition) represented the brief (15–20 s) period before the onset of REM sleep when the EEG displayed a mixture of delta and theta activity. REM sleep was identified by the presence of regular EEG theta activity coupled with low EMG relative to slow-wave sleep and a sleeping posture. The resolution and field of view of the video camera made it difficult to detect the phasic aspects of REM sleep such as muscle twitches or vibrissae movement.

Analysis of Ca^{2+} fluorescence during natural sleep–wake bouts and exploratory behavior. From the EEG, EMG, and video recording, clear episodes of quiet waking, NREM sleep, pre-REM sleep (REM transition), and REM sleep were identified based on the criteria described above (Neuroexplorer). The video was essential in identifying clear episodes of walking, eating, grooming, rearing, and digging. Not all mice engaged in these waking behaviors. During the test with novel objects, video recording was used to identify when the animals were exploring the objects. The entire bout of REM sleep was sampled as a single episode of REM sleep. Pre-REM sleep episodes represented the period (15–20 s) just before the start of REM sleep when the EEG displayed a mixture of delta and theta activity. NREM episodes that were sampled were distributed throughout NREM sleep with the sampling length being similar to the length of the individual REM sleep bout. We identified episodes of quiet waking based on EEG-EMG and video behavior during the recording period. A researcher (P.S.) blind to the Ca^{2+} imaging data selected the sampling episodes corresponding to the specific sleep–wake behavior.

The Ca^{2+} fluorescence data were analyzed by a researcher (C.B.-C. or S.L.) blind to the sleep–wake behavior data. The fluorescence signals were expressed as a *z*-score in 1 s bins without knowledge of and regardless of the sleep–wake behavior. After the sleep–wake behavior and the fluorescence data were analyzed, the two datasets were merged so that the rows represented time (1 s increment), one column represented the sleep–wake behavior (quiet waking, NREM, pre-REM, REM sleep, dig, eat, groom, rear, explore), and the other columns represented the fluorescence in individual neurons in each mouse. In each mouse, the average fluorescence (*z*-score) in each neuron during quiet wake, NREM, pre-REM, REM sleep, eating, grooming, walking, digging, rearing, and exploration was determined and plotted.

Analysis of the time course of Ca^{2+} fluorescence during transitions between sleep–wake states. In each mouse, the transition periods between sleep–wake states were identified, and the average fluorescence (*z*-scores) was determined. To determine the temporal progression of the Ca^{2+} signal during NREM sleep, we sampled the 30 s period before transitioning to 120 s of NREM sleep. We sampled 120 s of NREM sleep during the transition from quiet waking to NREM to better identify the change in fluorescence as sleep progressed. The transition from NREM to pre-REM sleep (REM transition) represents 15 s of NREM sleep that transits to 15 s of pre-REM sleep. For transitions to REM sleep, we identified the 15 s of pre-REM sleep that progressed into REM sleep. The transition from REM sleep to waking represented the 30 s of the REM sleep bout and the subsequent 15 s in quiet wake. The length of the transition periods was selected to properly convey the temporal pattern of the change in fluorescence across the various sleep states.

Cross-correlations. To examine the temporal dimension of the calcium dynamics in MCH neurons, single episodes of REM sleep were plotted for each mouse. Four mice that had the most extracted neurons were selected. In these four mice, in REM sleep there were 84 neurons of an overall total of 106 neurons. For each neuron, the calcium signal (*z*-score) was smoothed (loess method), and then normalized as a percentage of the maximum fluorescence *z*-score of the neuron. The *z*-scores that were used here were the same as those previously calculated to obtain average and maximum fluorescence response for each sleep state (0.1 s sampling rate). The calcium signals obtained during exploratory behavior (56 neurons) were also plotted.

To determine the spatial–temporal map, one matrix determined the cross-correlation coefficients of the fluorescence signal (temporal scale) while a second matrix tabulated the distance between the neurons in the field of view of the GRIN lens (spatial scale). The Pythagoras theorem calculated neuronal distances using Cartesian coordinates where the center of the neuron on the maximum projection frame was used to mark its (*x*,*y*) position. A script was developed (MatLab; S.O.) to combine the temporal and spatial matrices to represent a 2D spatial connectivity map. Spatial activity maps were created for REM sleep and for exploration of novel objects. The size of the circular symbol representing the neurons on the maps is denoted by the weight of significant (≥95% CI) cross-correlation links using $r \geq 0.60$ as the cutoff threshold. To reveal connection clusters, connectivity links were color coded from threshold ($r \geq 0.6$) to a perfect correlation ($r = 1.0$). Moreover, to determine whether distances among all neurons may relate to synchronicity, a Pearson correlation analysis was performed (GraphPad Prism 8.0, GraphPad Software). To strengthen the correlation analysis, distances were randomized. Pearson correlations were performed for each mouse and condition (REM sleep and exploration). Finally, to determine whether there was a difference in synchronicity between conditions for all cross-correlation values and the number of neuronal pairs, group averages (± SEM) were calculated, plotted, and statistically tested.

Postmortem analysis of GCaMP6 expression. The mice were anesthetized with 5% isoflurane and perfused transcardially with 0.9% saline (10 ml) followed by 10% buffered formalin in 0.1 M PBS (30 ml). The brains were collected and fixed in 10% buffered formalin for 1 week. The brains were equilibrated in 30% sucrose solution in 0.1 M PBS and cut coronally at 40 μm in one to four series. For MCH immunofluorescence staining, the sections were washed in 0.1 M PBS and blocked with 2% normal donkey serum for 30 min. The floating sections were incubated overnight with rabbit anti-MCH primary antibody (1:1000 dilution; catalog #H-070-47, Phoenix Pharmaceuticals; RRID:AB_10013632) at room temperature. The sections were washed in 0.1 M PBS and incubated for 2 h in donkey anti-rabbit Alexa Fluor 568-conjugated secondary antibody (1:500; catalog #A10042, Thermo Fisher Scientific; RRID:AB_2534017). The sections were washed and mounted onto gelatin-coated slides and coverslipped using fluorescence mounting medium. The fluorescence images were obtained at 10× and 20× using a Leica TCS-SP8 Confocal Microscope. The MCH immunopositive neurons (in red; Alexa Fluor 568) infected with AAV-DJ-EF1a-DIO-GCaMP6s virus specifically expressed enhanced yellow fluorescent protein (EYFP; in green). The colocalization of MCH-immunoreactive and EYFP was confirmed by 3D view software of *z*-stack scan.

←

(*Figure legend continued.*) immunopositive for MCH. The coronal sections were incubated with the MCH antibody and visualized using a Leica confocal microscope. Scale bar, 80 μm. ***D***, The field of view of the GRIN lens with fluorescence ($\Delta F/F_0$) in somata and processes during REM sleep in neurons extracted automatically by PCA-ICA analysis. We have labeled the three neurons (labeled 1, 2, and 3) whose Ca^{2+} fluorescence is plotted in ***E***. ***E***, GCaMP6s fluorescence ($\Delta F/F_0$) in MCH neurons is associated with REM sleep. Ca^{2+} imaging was performed simultaneously with recording of cortical EEG and EMG activity in the nuchal muscles. Behavioral video recordings were obtained and examined to identify behaviors such as walking, eating, grooming, or eating. Activity in the EEG (depicted as power spectra, 0.3–15 Hz) and the EMG is used to identify wake, NREM, and REM sleep states (labeled as hypnogram). The traces depict the change in fluorescence ($\Delta F/F$) during wake–sleep bouts of the three neurons identified in ***D***. In each neuron, the $\Delta F/F_0$ (expressed as a *z*-score) varies with the wake–sleep state of the animal, with peak fluorescence associated with REM sleep. The hypnogram categorizes the sleep–wake states in the following colors: purple, active wake; blue, quiet wake; green, NREM; yellow, pre-REM sleep; red, REM sleep. ***F***, The same field of view as in ***D***, but this image shows the PCA-ICA extracted neurons ($\Delta F/F_0$) while the mouse was engaged in exploring novel objects placed in its home cage. This image shows that some neurons that were evident in REM sleep (***D***) were also activated during exploratory behavior. However, some neurons in ***D*** were not evident during exploratory behavior, indicating selective activation of these neurons during REM sleep (***D***). Thirty percent of the neurons were activated during REM sleep but not during exploratory behavior, indicating that a subset of MCH neurons is selectively active in REM sleep. ***G***, GCaMP6s fluorescence in MCH neurons while exploring novel objects. The traces are from the same neurons represented in REM sleep (***E***). Note that the GCaMP6s has a rapid response and a slow rate of decay, which makes it difficult to infer whether the imaged neuron fired as single spikes or in clusters.

Table 1. Summary table of the sex, type of calcium indicator (GCaMP6), number of MCH neurons and sampling parameters that were used to identify change in Ca^{2+} fluorescence in MCH neurons

Mouse ID	GCaMP	Number of neurons	QW	NREM sleep	Pre-REM	REM sleep	Eat	Groom	Walk	Dig	Rear	Explore
Number of samples												
F18	Slow	1	12	13	4	4						
F22	Slow	15	6	9	5	5	1	1	2	1	3	7
F29	Slow	2	3	12	2	2	1	1	5	1	1	22
F33	Slow	25	10	13	5	3	1	2	4		3	12
F35	Slow	22	9	14	9	5	2	1	4		3	15
M39	Slow	23	4	12	7	6		3	2		2	13
M42	Slow	6	7	13	6	5			2		2	19
F41	Medium	6	5	11	3	3			4		14	5
M61	Medium	4	4	15	2	2	2	3	5		1	6
M62	Medium	3	5	18	7	4		1	5		6	6
Total		107	65	130	50	39	7	2	33	2	35	105
Mean sample length (s)												
F18	Slow	1	11.8	25.5	17.7	47.4						
F22	Slow	15	55.5	86.4	19.4	58.6	106.0	47.2	26.3	93.2	3.4	12.0
F29	Slow	2	80.1	145.6	17.8	129.4	127.1	103.3	11.78	99.1	1.9	8.4
F33	Slow	25	21.8	79.8	20.0	47.3	61.6	71.6	43.5		3.5	8.0
F35	Slow	22	29.9	100.7	15.5	66.9	44.2	58.6	90.8		3.9	6.1
M39	Slow	23	24.4	69.6	15.8	65.6		33.4	8.3		6.1	18.3
M42	Slow	6	19.1	60.6	18.0	36.3			63.0		8.0	10.7
F41	Medium	6	29.2	65.3	16.6	73.1			8.3		7.4	10.6
M61	Medium	4	17.0	48.0	15.0	130.5	9	84.8	58.3		12	18.3
M62	Medium	3	36.7	56.5	14.9	39.7		15.0	36.8		13.2	4.8
Mean ± SEM			32.6 ± 6.5	73.8 ± 10.3	17.1 ± 0.6	69.5 ± 10.8	69.6 ± 15.0	59.1 ± 9.6	38.6 ± 9.0	96.1 ± 1.3	6.6 ± 1.2	10.8 ± 1.5

A total of 107 MCH neurons were recorded, but 1 neuron from mouse F35 was excluded since its average fluorescence in REM sleep was twice as high as the next data point. The mice were 171.4 ± 27.72 d old, weighed 36.04 ± 3.81 g, and were maintained on a 12 h light/dark cycle (23 °C) with *ad libitum* access to food and water. Mature mice were examined to be able to support the weight of the single-photon miniscope (nVISTA; Inscopix). The EEG, EMG, and video recordings were used to identify clear episodes of the sleep–wake behavior noted in the first row. Not all mice engaged in the waking behaviors. During the test with novel objects, video recording was used to identify when the animals were exploring the objects. The entire bout of REM sleep was sampled as a single episode of REM sleep. The sex of the mice is identified in the first column. F, Female; M, male.

Experimental design and statistical analysis. The mice were tested in a repeated-measures design where the dependent variable was the Ca^{2+} fluorescence (z-score) in each neuron, the between-subjects variable was mouse by neuron, and the within-subjects variable were the repeated measures of the independent variables (quiet wake, NREM, pre-REM sleep, REM sleep, walk, dig, groom, eat, rear, and explore). A generalized linear mixed model (GLMM; SPSS 25, IBM) with *post hoc* Bonferroni paired comparisons (sequential adjusted) was used to compare the fixed and random effects of the repeated measures (wake–sleep states and behavior). An unstructured covariance matrix yielded a low Akaike information criteria and the best model fit. The GLMM model was appropriate based on the correlation of the fluorescence data between the neurons, the skewed distribution of the data (Kolmogorov–Smirnov test for normality), and unbalanced design. Statistical significance was evaluated at the $p = 0.05$ level (two tailed). Graphs were plotted using GraphPad Prism (GraphPad Software).

Data and material availability. All raw and extracted data, code, and materials used in the study are available by writing to the corresponding authors. We are happy to share the raw data and encourage data mining of the imaging dataset to extend the analysis.

Results

In vitro slice electrophysiology and GCaMP6 fluorescence of MCH neurons

A brain slice electrophysiology/imaging experiment showed that the depolarization of MCH neurons transduced with GCaMP6s resulted in increased fluorescence (Fig. 1). GCaMP6s-expressing MCH neurons in brain slices from MCH-Cre mice were recorded in the whole-cell configuration and imaged. GCaMP6s fluorescence ($\Delta F/F$) increased in response to an injection of depolarizing current that evoked spikes (Fig. 1*A*). There was a positive correlation between the change in GCaMP6s fluorescence and the number of spikes (Fig. 1*B*). This is the first direct confirmation that changes in GCaMP6 fluorescence in MCH neurons reflect an increase in spiking.

Calcium during sleep and wake

Next, we recorded cytoplasmic Ca^{2+} levels in MCH neurons during sleep, and also during periods of activity such as walking, grooming, rearing, eating, and exploration of novel objects. In 10 MCH-Cre mice, microinjections of the Ca^{2+} indicator (rAAV-DJ EF1a-DIO-GCaMP6s or -GCaMP6m) were made into the lateral hypothalamus where the MCH neurons are located. Our data from postmortem imaging of mouse brains cleared by the CLARITY method (Shiromani and Peever, 2017) was critical in enabling the correct positioning of the GRIN lens atop clusters of MCH neurons, allowing us to maximize the number of MCH neurons that were imaged (Fig. 2*A*–*C*).

GCaMP6 fluorescence signals were automatically extracted from individual MCH neurons in each MCH-Cre mouse using PCA-ICA. Each MCH neuron could be tracked over time based on size, shape, and location (Fig. 2*D*,*E*). For data analysis, the average fluorescent signal associated with each neuron was represented as a z-score and plotted as a trace in relation to sleep–wake states and behavior (Fig. 2*E*,*G*). A total of 107 individual neurons were imaged. One neuron from mouse F35 was excluded from the analysis as an outlier since its z-score ($z = 7.82$) during REM sleep was approximately twofold above the other data. Table 1 summarizes the number of neurons recorded, the sex of the mice, and the slow versus medium type of the GCaMP6 that was used. The general linear mixed model revealed no significant difference between sex or between slow versus medium types of GCaMP6.

To identify changes in fluorescence during specific sleep–wake behaviors a number of samples were taken during periods

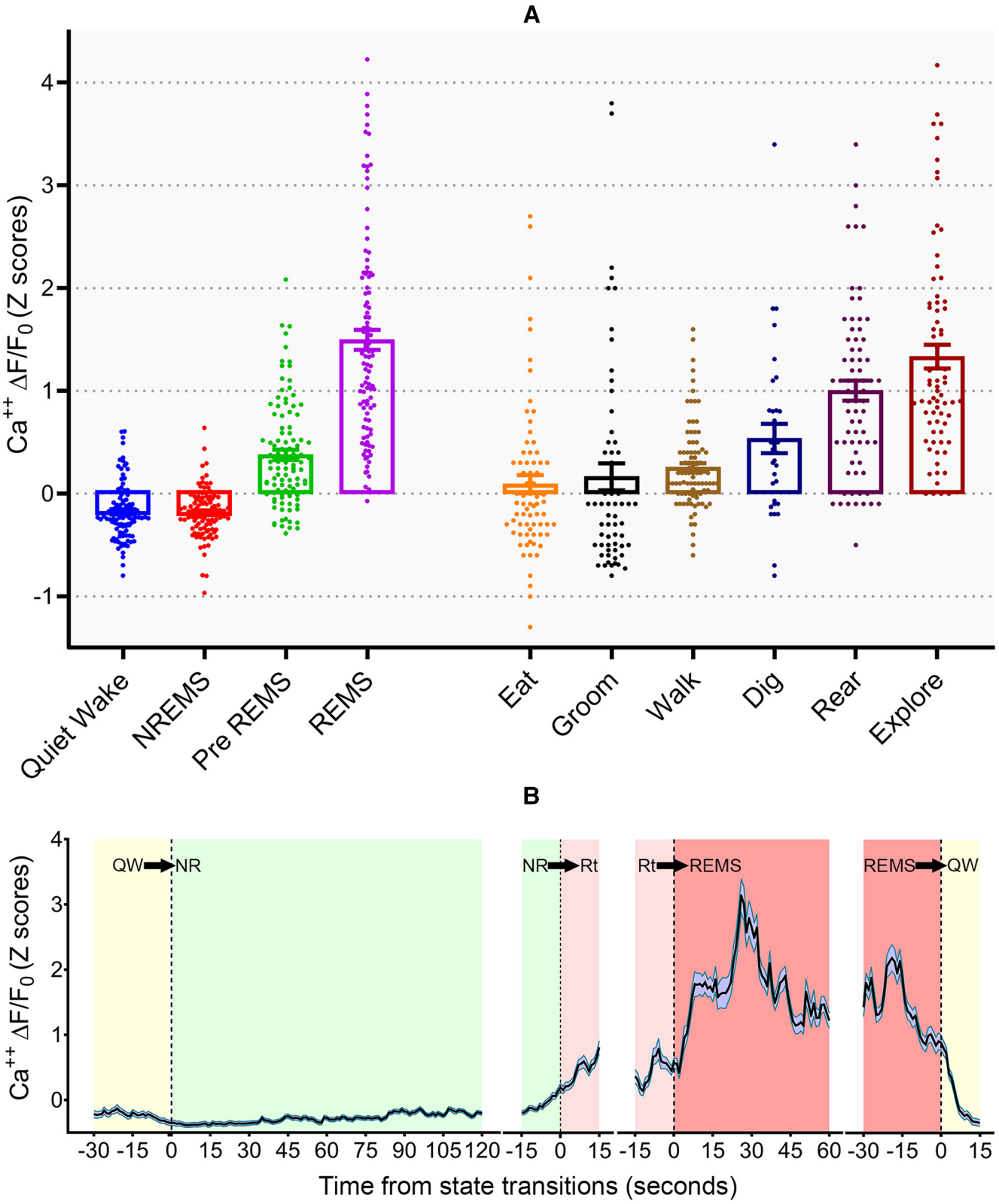

Figure 3. Average fluorescence ($\Delta F/F_0$) in MCH neurons is highest during REM sleep and exploratory behavior. ***A***, Average change in fluorescence ($\Delta F/F_0$ expressed as *z*-scores) in MCH neurons across wake–sleep states and wake behaviors in MCH-Cre mice. A total of 107 distinct neurons in 10 MCH-Cre transgenic mice was extracted automatically by the Mosaic software (Inscopix). Fluorescence in one neuron was twofold higher during REM sleep compared with the next data point, and it was excluded from the data analysis. Each data point represents the average fluorescence (*z*-score) of individual neurons in samples taken during the specific sleep–wake behavior. Table 1 summarizes the number of neurons recorded in each of the 10 mice. Table 1 also summarizes the number and length of the samples for each sleep–wake behavior represented in the bar graph. Each box in the bar graph summarizes mean and SE, and depicts data points representing individual neurons. The number of MCH neurons represented in each bar is as follows: first four bars = 106; eat = 72; groom = 61; walk = 92; dig = 33; rear = 71; explore = 74. A GLMM design was used based on the correlation of the fluorescence data between the neurons, the skewed distribution of the data (failed Kolmogorov–Smirnov test for normality), and unbalanced design. Pairwise comparisons were made with the Bonferroni *post hoc* test (sequential adjusted). There was a significant increase in Ca^{2+} activity during REM sleep compared with quiet wake, NREM, and pre-REM sleep ($p < 0.001$). Fluorescence in pre-REM sleep was significantly higher than quiet wake or NREM ($p < 0.001$). When the mice engaged in behaviors involving (*Figure legend continues.*)

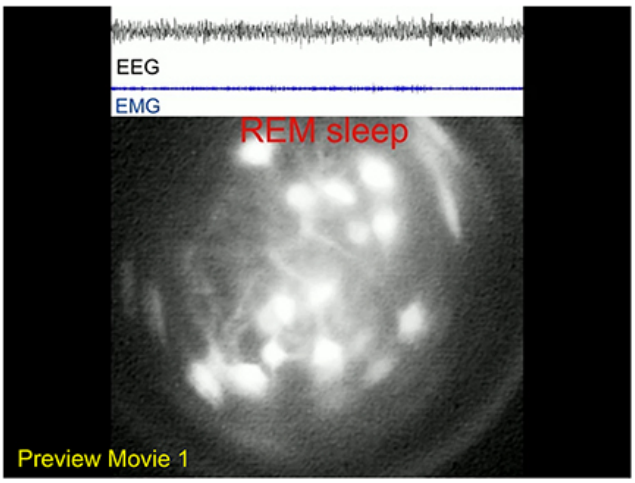

Movie 1. Calcium fluorescence in hypothalamic MCH neurons during REM sleep in freely behaving MCH-cre mice. A single-photon miniscope (Inscopix) recorded calcium fluorescence (10 fps movie), while the sleep–wake state of the animal was identified by recording the EEG and EMG (Plexon). REM sleep was identified by the presence of theta waves in the EEG and a low EMG relative to waking. The movie was condensed and accelerated from a recording session (33 min and 26 s) when several REM sleep bouts were evident. The movie shows that during REM sleep, MCH neurons exhibit synchronized phasic activity. This is the first evidence of synchronous activation of a single phenotype of neurons.

of natural sleep and quiet wake, and while the animals were engaged in specific wake behaviors. Table 1 summarizes the number and length of samples that were taken in each mouse. GCaMP6 fluorescence from individual MCH neurons significantly increased with REM sleep (general linear mixed model: $F_{(3,384)} = 34.612$; $p = 0.0001$; Movie 1). Average GCaMP6 fluorescence was highest during REM sleep while the nadir was during quiet waking and NREM sleep (sequential Bonferroni *post hoc* tests; Fig. 3*A*). Even when the mice were engaged in overt behaviors involving gross locomotor activity such as walking, eating, digging, or grooming, the GCaMP6 fluorescence was significantly less than in REM sleep (sequential Bonferroni, $p < 0.02$; Fig. 3*A*). Mean GCaMP6 fluorescence during walking, eating, digging, and grooming was not significantly different from each other (sequential Bonferroni). Interestingly, following the introduction of novel objects in the home cage, we found that when the mice engaged in rearing behavior (stood on their hindlegs), there was an increase in GCaMP6 fluorescence that was not significantly different from that during REM sleep (sequential Bonferroni, $p < 0.065$; Fig. 3*A*). Thus, GCaMP6 fluorescence in at least one waking behavior, one associated with exploration and novelty (Lever et al., 2006), is similar to that in REM sleep. This observation was unexpected since MCH neurons are believed to be active only in sleep (Hassani et al., 2009).

To determine more closely the time course of the change in fluorescence, we examined the transition periods (1s epochs) between wake–sleep states (Fig. 3*B*). The fluorescence began to progressively increase from NREM to the pre-REM sleep period (15 s before start of REM sleep) and peaked midway into REM sleep. There was a decline in the signal just before the onset of waking (Fig. 3*B*). The fluorescence signal corroborates the pattern of electrophysiological activity of the MCH neurons (Hassani et al., 2009).

Orchestration of MCH neuron activity

Next, we determined the pattern of fluorescence among the recorded neurons. During REM sleep, GCaMP6 fluorescence occurred in phasic bursts in all animals. To study the synchronous pattern of the volleys, we examined four mice where most MCH neurons were recorded (neurons: 84 of 106 in REM sleep; and 56 of 106 in exploration; Fig. 4*A*). We determined that the individual volleys were highly temporally correlated ($r = 0.92$) among the MCH neurons (Fig. 4*A*). Waves of Ca^{2+} volleys began to emerge at the start of REM sleep and the temporal pattern indicates that the fluorescence in the MCH neurons occurs simultaneously rather than sequentially. We did not find that the Ca^{2+} volleys in the MCH neurons were correlated with theta, slow-wave ripples or up-down states in the cortex.

To identify the spatial pattern of activation of the MCH neurons during REM sleep, we determined the relationship between the change in fluorescence among pairs of MCH neurons as a function of the distance between them. There was a weak relationship between the fluorescence and distance between the neurons ($r = 0.13$). A spatial activity map summarizes the pattern of activation between distal and proximal MCH neurons in the field of view (Fig. 5). During REM sleep, fluorescence changes in many MCH neurons were strongly correlated ($r \geq 0.6$; $p < 0.01$) with those in other MCH neurons, indicating the ensemble activation of an MCH neural network during REM sleep. This is the first study to document a dynamic pattern of activation of multiple neurons of the same phenotype during REM sleep.

Having derived a pattern of activation of MCH neurons during REM sleep, we asked whether other behaviors would also trigger a similar pattern. Therefore, we monitored the MCH neurons during periods of exploratory behavior. Another study used fiber photometry to suggest that MCH neurons may be activated by sensory stimuli and novel object exploration (González et al., 2016); whereas fiber photometry cannot distinguish between individual cells, the miniscope provides spatial (distance between neurons in the field of view) as well as cellular resolution.

Following the sleep recordings, the mice were given novel objects to explore for 10 min. Figure 2*F* depicts the same field of view of the GRIN lens as in REM sleep (Fig. 2*D*). Figure 2*G* depicts the changes in Ca^{2+} of three neurons during the exploration period (Fig. 2*G*). During the exploration session, some neurons that were excited in REM sleep were not fluorescent (Fig.

←

(*Figure legend continued.*) gross locomotor activity (eat, groom, walk, or dig), the fluorescence was significantly lower compared with REM sleep. However, during rearing behavior or exploration of novel objects, the fluorescence was not significantly different from REM sleep. Thus, a subset of the MCH neurons (69.8%; 74 of 106 neurons) was also as active during exploratory behavior as in REM sleep. ***B***, Time course of change in fluorescence ($\Delta F/F_0$, expressed as *z*-scores) during the transition from quiet wake (QW) to NREM to pre-REM to REM sleep to QW. The sleep and the imaging data were analyzed separately in a blind manner, and the two datasets were combined once PCA-ICA analysis had established the *z*-scores. The figure summarizes the average fluorescence of MCH neurons ($n = 106$) in 1.0 s epochs during the transition periods between sleep states. The fluorescence began to increase 30 s after the onset of NREM sleep and peaked midway into the REM sleep bout. The time course of increase in fluorescence during NREM and REM sleep is similar to the pattern of action potentials of MCH neurons (Hassani et al., 2009). In that study (Hassani et al., 2009), the rate of action potentials of single MCH neurons during REM sleep was 12 Hz. In the present study, Ca^{2+} fluorescence occurred in volleys during REM sleep indicating the high rate of activity of the underlying MCH neurons (Movie 1). The steady progression of the fluorescence suggests that optogenetic stimulation of the MCH neurons during NREM sleep should further depolarize the MCH neurons and increase NREM sleep, which it does in both mice and rats (Konadhode et al., 2013; Blanco-Centurion et al., 2016). Optogenetic stimulation during the pre-REM sleep period should trigger REM sleep, which it does (Jego et al., 2013). Stimulation during REM sleep should not prolong the REM sleep bout, which is also consistent with published data (Jego et al., 2013).

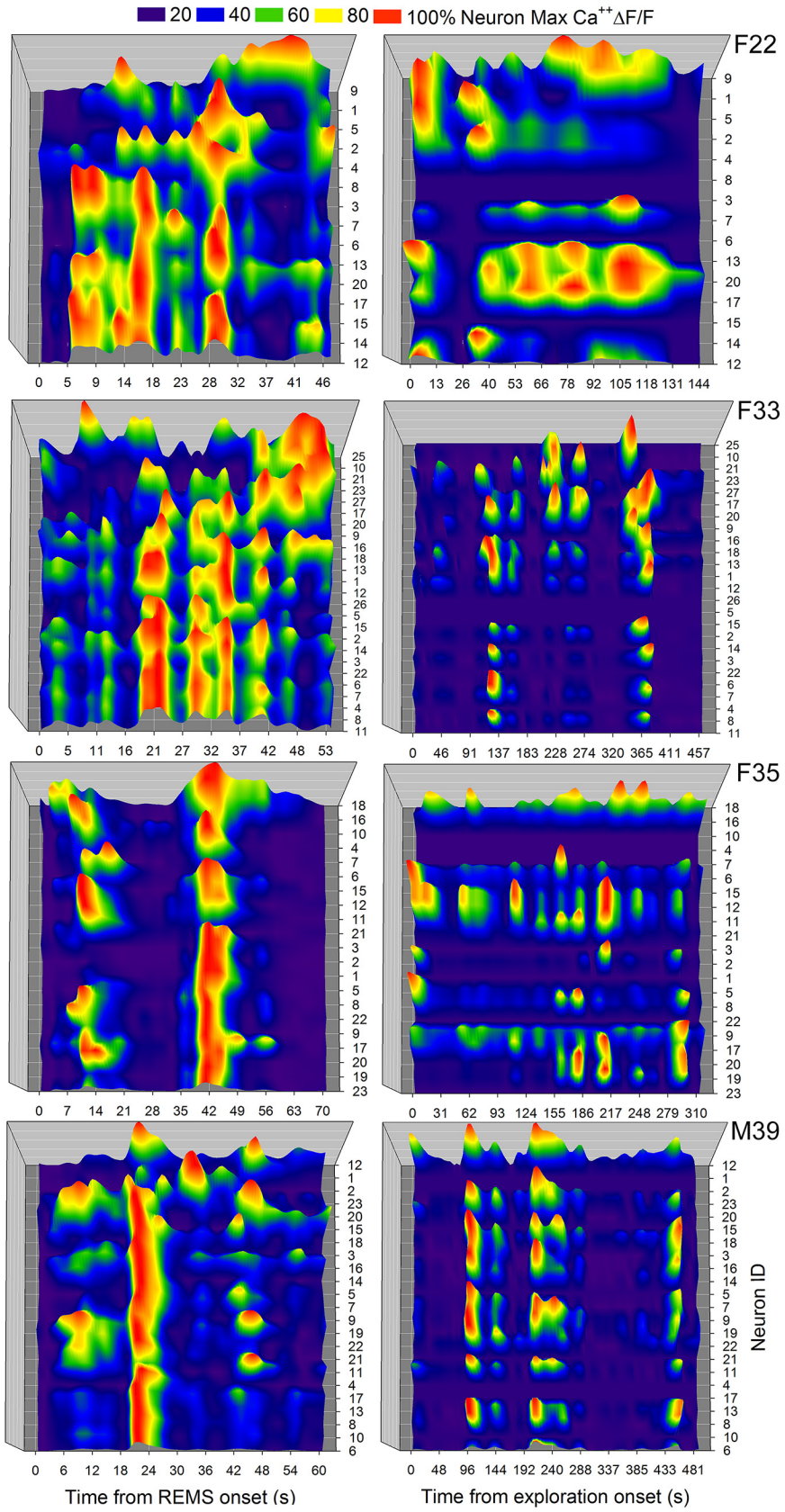

Figure 4. Fluorescence in MCH neurons occurs in synchronous volleys during REM sleep and exploratory behavior. To identify the temporal pattern of the fluorescence peaks across the MCH neurons, the Ca^{2+} traces (expressed as *z*-score) were plotted during individual bouts of REM sleep (left) and exploratory behavior (right). The spatial location of the neurons in the GRIN lens field of view is depicted in Figure 5. The four MCH-Cre mice with the most MCH neurons were plotted (Table 1). In the four mice, there were 84 of 106 neurons in REM sleep and 56 of 106 neurons in exploration. Each line represents the change in Ca^{2+} fluorescence (shown as a contour heat map with red indicating maximum) in individual neurons (*y*-axis) across time (*x*-axis; 1.0 s epochs) during REM sleep and exploratory behavior. In each animal, the neurons are sorted based on the strength of the correlation of fluorescence peaks between pairs of neurons during REM sleep; neurons with the most pairwise correlation are at the bottom. While this figure depicts the temporal relationship of fluorescence between neurons, Figure 5 depicts the spatial location of the neurons within the GRIN lens field of view. During exploratory behavior, a subset of MCH neurons was not activated, and the trace of the neurons does not appear in the right panel. There was high correlation in the change in fluorescence among the MCH neurons in each animal during REM sleep ($r = 0.96$, df = 15; $r = 0.98$, df = 25; $r = 0.85$, df = 21; $r = 0.90$, df = 23) vs exploratory behavior ($r = 0.7$, df = 11; $r = 0.76$, df = 16; $r = 0.70$, df = 13; $r = 0.71$, df = 16), indicating synchronous activity.

2*D*,*F*). We found that of the 106 MCH neurons that were activated during REM sleep, 69.8% (74 of 106 neurons) also showed increased fluorescence during novel object exploration. Average fluorescence during exploration was not significantly different from that during REM sleep or rearing behavior (GLMM, $F = 0.25$; df = 2, 239; not significant; Fig. 3*A*). When the novel objects were presented, mice engaged in behaviors associated with exploration and novelty, such as rearing and sniffing (Lever et al., 2006). We did not find any MCH neurons that were selectively active only in exploratory behavior, while the remaining 32 MCH neurons (30.19%) were selectively active only during REM sleep ($\chi^2 = 49.19$; df = 2; $p < 0.001$). Thus, a subset of MCH neurons was selectively active only during REM sleep. Figure 4*B* indicates that during exploratory behavior multiple MCH neurons were activated simultaneously and in a phasic manner ($r = 0.72$; Fig. 4*A*), similar to that during REM sleep ($r = 0.92$, rank sum test). The average fluorescence increased when the mice investigated the objects by rearing and sniffing (Movie 2). Figure 5 summarizes the spatial network map of the MCH neurons during exploratory behavior and shows fewer strong associations between pairs of MCH neurons. To quantify the change in network behavior, we computed pairwise correlation coefficients for all pairs of neurons during REM sleep versus exploratory behavior and determined that the magnitude of MCH network activation during exploratory behavior (mean correlation coefficient = 0.43) was significantly less compared with REM sleep (mean correlation coefficient = 0.54; rank sum test = 3.037; df = 56; $p < 0.002$).

Discussion

The primary observation of this study was that all of the recorded MCH neurons had

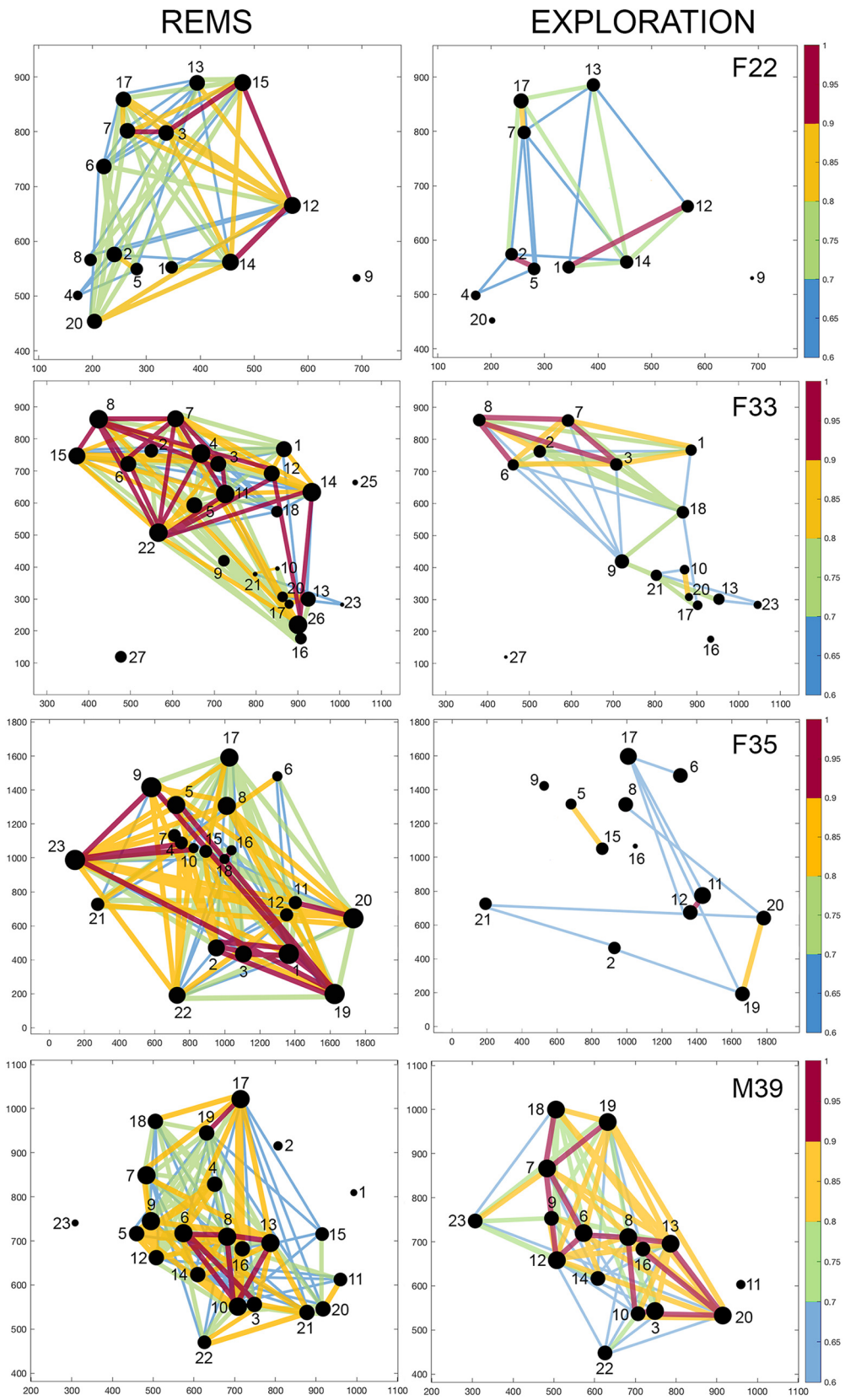

Figure 5. Spatial activation of MCH neurons during REM sleep and exploratory behavior. Spatial correlograms showing the relationship of the fluorescence between MCH neurons during REM sleep and exploratory behavior. The fluorescence data are from the same four mice depicted in Figure 4. Lines connecting neuronal pairs are colored to reflect the strength of the correlation coefficient ($r = 0.6–1.0$). The number of associations between pairs of neurons is denoted by the size of the neurons (larger diameter = more associations). Each panel depicts the extracted neurons in the field of view of the GRIN lens, with each neuron plotted along its x and y coordinates in the GRIN lens field of view. During REM sleep, there are more associations between MCH neurons indicating a more complete activation of the MCH neuronal network compared with exploratory condition (rank sum test). Such maps provide a heuristic basis for comparing network activation in two different conditions.

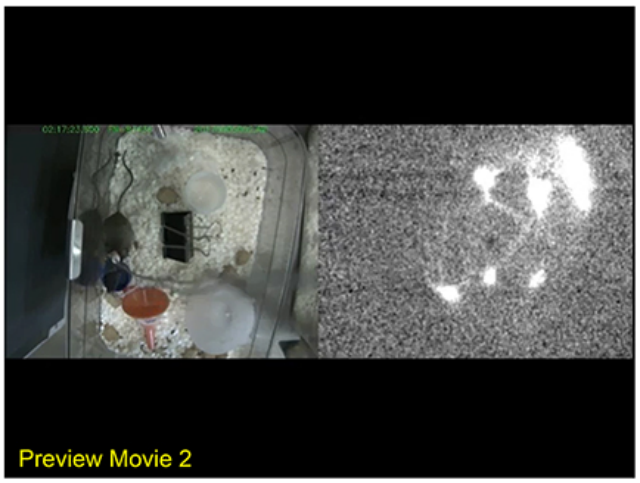

Movie 2. Calcium fluorescence in hypothalamic MCH neurons during exploration of novel objects. The same neurons that were depicted in Movie 1 were recorded while the mouse explored novel objects. The movie was condensed and accelerated from a recording session (306 s). During the test with novel objects, many MCH neurons that were active in REM sleep were also active during exploratory behavior. Overall, the tally of the 106 MCH neurons from 10 MCH-cre mice (6 females) revealed that 70% of the MCH neurons were active in both REM sleep and exploratory behavior, while 30% were active only in REM sleep. Activation of the MCH neurons may form a memory trace of salient survival cues.

the highest GCaMP6 fluorescence during REM sleep relative to quiet waking or NREM sleep, corroborating for the first time the electrophysiology study in head-restrained rats (Hassani et al., 2009). Our study breaks new ground by discovering that 70% of the MCH neurons were also activated during exploratory behavior, but 30% were active only in REM sleep. In freely behaving mice, the fluorescence in individual MCH neurons progressively increased from quiet waking to NREM, with a peak during REM sleep (Fig. 3*B*). The sleep-related time course of the fluorescence signal corroborates the pattern of electrophysiological activity of the MCH neurons noted in head-restrained rats (Hassani et al., 2009). The rising pattern of the signal during sleep indicates that these neurons can be activated to induce sleep (Jego et al., 2013; Konadhode et al., 2013; Tsunematsu et al., 2014; Blanco-Centurion et al., 2016). Because the fluorescence signal is in individual neurons that can be mapped along a spatial and temporal scale, we discovered that during REM sleep there was ensemble activation of the MCH neurons in the field of view (Figs. 4, 5). This is the first evidence of concurrent activation of multiple neurons of the same phenotype during REM sleep.

In the *in vitro* study, we confirmed that the fluorescence signal in the MCH neurons transfected with GCaMP6s was strongly linked to depolarization and the generation of action potentials of the neuron (Fig. 1), thereby validating the Ca^{2+} fluorescence in MCH neurons in the freely behaving mice. We used GCaMP6 (slow or medium) to monitor the change in intracellular Ca^{2+} because of its speed, very high sensitivity, intensity, and durability of the fluorescent signal (Chen et al., 2013). Both types of GCaMP6 have a similar peak response time to a depolarizing signal that triggers a single action potential, but the fluorescent signal of GCaMP6s takes 1.5 s to decay compared with 1.0 s for GCaMP6m (Chen et al., 2013). GCaMP6f (fast) has a decay time of 0.5s but is still too slow for detecting single spikes beyond 2 Hz. In the *in vivo* study, the medium type of GCaMP6 was used because we exhausted our supply of GCaMP6s. There was no significant difference in Ca^{2+} fluorescence between the two types of Ca^{2+} indicators. Because of the slow time course of the decay of the fluorescent signal, it is difficult to infer whether the imaged neuron fired as single spikes or in clusters. Newer voltage sensors or next-generation GCaMP might be able to resolve the temporal pattern of imaged neurons (Bayguinov et al., 2017).

Microendoscopy has been used to image the activity of various phenotypes of brain neurons during quiet waking and sleep (Weber et al., 2015, 2018; Cox et al., 2016; Chung et al., 2017; Chen et al., 2018). We took advantage of the versatility of the miniscope by also imaging the same neurons while the mice were exploring novel objects and discovered that 70% of the MCH neurons that were active in REM sleep were also active during the exploration of novel objects. During exploratory behavior and REM sleep the Ca^{2+} signal occurred in phasic bursts synchronized across the imaged neurons (Figs. 4, 5). During exploratory behavior, the Ca^{2+} signal in specific MCH neurons is likely to be based on input from sensory and motor circuits (González et al., 2016). However, during REM sleep, a time when the brain is considered to be as active as in waking, such sensory input is lacking, but the MCH neurons were activated synchronously. The mechanism responsible for the activation of the MCH neurons during REM sleep may be a result of the silence in activity of the arousal neurons (Aston-Jones and Bloom, 1981; John et al., 2004; Wu et al., 2004; Lee et al., 2005; Mileykovskiy et al., 2005). However, now that MCH neurons have been discovered to also be active in waking, what is the interplay between the MCH and arousal neurons? In waking, there might still be a reciprocal relationship between the MCH and arousal neurons just as it is in sleep as suggested by a fiber-photometry study that found that during exploratory behavior the MCH neurons become active once the activity in the orexin neurons subsides (González et al., 2016). However, to get a clearer understanding of the interplay between the orexin and MCH neurons, both of these neurons need to be imaged simultaneously with a single-cell resolution in freely behaving animals. Thus, new imaging tools will be required to track activity of both the orexin and MCH neurons simultaneously.

What might be the functional effect of the activation of MCH neurons? The accumulation of Ca^{2+} was detected in the MCH somata including its processes (Fig. 2*D*,*F*). We only analyzed the change in Ca^{2+} fluorescence in the MCH somata but, considering that increased Ca^{2+} in the somata and processes has been linked to action potentials and neurotransmitter release (Neher and Sakaba, 2008; Chen et al., 2013), the activated MCH neurons may well have influenced their downstream targets. We found that Ca^{2+} in the MCH neurons begins to increase in NREM sleep (Fig. 3*B*) and then there is a steep Ca^{2+} increase in these neurons just before REM sleep. Peak Ca^{2+} occurred in REM sleep (Fig. 3*B*) and 70% of these neurons were activated while exploring novel objects. Activated MCH neurons may stimulate memory consolidation through MCH receptors on downstream targets such as the hippocampus. Mice lacking MCH receptor 1, the only MCH receptor that is present in rodents, have impaired long-term potentiation in hippocampal CA1 pyramidal cells (Pachoud et al., 2010). Activation of the hypothalamic MCH neurons while exploring novel objects may convey salient cues related to survival, such as food source, and facilitate memories to be formed. The activation of the MCH neurons during REM sleep may induce a brain state conducive to replaying the novel information that then serves to strengthen the memory trace (Chen and Wilson, 2017).

The versatility of the miniscope allows the same neurons whose phenotype is known to be followed longitudinally and under various conditions in freely behaving mice. Our study

more rigorously tested the behavior of the same MCH neurons in sleep and in a novel condition during active waking. We found that 70% of the MCH neurons were active in REM sleep and in conditions that require the cells to integrate new information. Other methods, such as immediate-early gene (e.g., c-Fos) expression (Shiromani et al., 1992; Sherin et al., 1996; Modirrousta et al., 2005; Verret et al., 2003) and functional MRI in humans (Kaufmann et al., 2016) are used to map activation of neurons or specific brain regions during waking, NREM sleep, and REM sleep. In contrast to these methods, Ca^{2+} imaging provides cellular resolution by mapping the time course of the fluorescence in individual neurons in the same animal. By mapping the spatial and temporal patterns of the fluorescence signal, we derived a network map of the activity of the MCH neurons during REM sleep and exploratory behavior (Fig. 5). We suggest that activation of these neurons represents an internal brain activation that is associated with REM sleep, a state that is similar to waking. In humans, a functional network is activated in REM sleep and is associated with dreaming (Chow et al., 2013). We have now identified a single phenotype of neurons in mice that displays network activation during REM sleep. A subset of these neurons was also activated during novel experience, and we suggest that their activation during REM sleep may be part of the oneiric replay of waking events. We suggest that a spatial map of the fluorescence signal at the neuronal level provides a heuristic basis for comparing network activation in different conditions and is a first step toward a sleep connectome. Since MCH neurons are present in all vertebrates (Nahon et al., 1989; Bittencourt et al., 1992), we suggest that MCH neurons can be imaged in animals other than rodents to determine whether a brain network indicative of REM sleep is periodically activated. This may more definitively identify whether MCH neurons in other vertebrate species function in a manner related to dreaming or REM sleep.

References

Aston-Jones G, Bloom FE (1981) Activity of norepinephrine-containing locus coeruleus neurons in behaving rats anticipates fluctuations in the sleep-waking cycle. J Neurosci 1:876–886.

Bayguinov PO, Ma Y, Gao Y, Zhao X, Jackson MB (2017) Imaging voltage in genetically defined neuronal subpopulations with a cre recombinase-targeted hybrid voltage sensor. J Neurosci 37:9305–9319.

Bittencourt JC, Presse F, Arias C, Peto C, Vaughan J, Nahon JL, Vale W, Sawchenko PE (1992) The melanin-concentrating hormone system of the rat brain: an immuno- and hybridization histochemical characterization. J Comp Neurol 319:218–245.

Blanco-Centurion C, Liu M, Konadhode RP, Zhang X, Pelluru D, van den Pol AN, Shiromani PJ (2016) Optogenetic activation of melanin-concentrating hormone neurons increases non-rapid eye movement and rapid eye movement sleep during the night in rats. Eur J Neurosci 44: 2846–2857.

Chen KS, Xu M, Zhang Z, Chang WC, Gaj T, Schaffer DV, Dan Y (2018) A hypothalamic switch for REM and non-REM sleep. Neuron 97:1168–1176.e4.

Chen TW, Wardill TJ, Sun Y, Pulver SR, Renninger SL, Baohan A, Schreiter ER, Kerr RA, Orger MB, Jayaraman V, Looger LL, Svoboda K, Kim DS (2013) Ultrasensitive fluorescent proteins for imaging neuronal activity. Nature 499:295–300.

Chen Z, Wilson MA (2017) Deciphering neural codes of memory during sleep. Trends Neurosci 40:260–275.

Chow HM, Horovitz SG, Carr WS, Picchioni D, Coddington N, Fukunaga M, Xu Y, Balkin TJ, Duyn JH, Braun AR (2013) Rhythmic alternating patterns of brain activity distinguish rapid eye movement sleep from other states of consciousness. Proc Natl Acad Sci U S A 110:10300–10305.

Chung S, Weber F, Zhong P, Tan CL, Nguyen TN, Beier KT, Hörmann N, Chang WC, Zhang Z, Do JP, Yao S, Krashes MJ, Tasic B, Cetin A, Zeng H, Knight ZA, Luo L, Dan Y (2017) Identification of preoptic sleep neurons using retrograde labelling and gene profiling. Nature 545:477–481.

Cox J, Pinto L, Dan Y (2016) Calcium imaging of sleep-wake related neuronal activity in the dorsal pons. Nat Commun 7:10763.

Cvetkovic V, Brischoux F, Jacquemard C, Fellmann D, Griffond B, Risold PY (2004) Characterization of subpopulations of neurons producing melanin-concentrating hormone in the rat ventral diencephalon. J Neurochem 91:911–919.

Elias CF, Saper CB, Maratos-Flier E, Tritos NA, Lee C, Kelly J, Tatro JB, Hoffman GE, Ollmann MM, Barsh GS, Sakurai T, Yanagisawa M, Elmquist JK (1998) Chemically defined projections linking the mediobasal hypothalamus and the lateral hypothalamic area. J Comp Neurol 402:442–459.

Ghosh KK, Burns LD, Cocker ED, Nimmerjahn A, Ziv Y, Gamal AE, Schnitzer MJ (2011) Miniaturized integration of a fluorescence microscope. Nat Methods 8:871–878.

González JA, Iordanidou P, Strom M, Adamantidis A, Burdakov D (2016) Awake dynamics and brain-wide direct inputs of hypothalamic MCH and orexin networks. Nat Commun 7:11395.

Hamel EJ, Grewe BF, Parker JG, Schnitzer MJ (2015) Cellular level brain imaging in behaving mammals: an engineering approach. Neuron 86:140–159.

Hassani OK, Lee MG, Jones BE (2009) Melanin-concentrating hormone neurons discharge in a reciprocal manner to orexin neurons across the sleep-wake cycle. Proc Natl Acad Sci U S A 106:2418–2422.

Jego S, Glasgow SD, Herrera CG, Ekstrand M, Reed SJ, Boyce R, Friedman J, Burdakov D, Adamantidis AR (2013) Optogenetic identification of a rapid eye movement sleep modulatory circuit in the hypothalamus. Nat Neurosci 16:1637–1643.

John J, Wu MF, Boehmer LN, Siegel JM (2004) Cataplexy-active neurons in the hypothalamus: implications for the role of histamine in sleep and waking behavior. Neuron 42:619–634.

Kaufmann T, Elvsåshagen T, Alnæs D, Zak N, Pedersen PØ, Norbom LB, Quraishi SH, Tagliazucchi E, Laufs H, Bjørnerud A, Malt UF, Andreassen OA, Roussos E, Duff EP, Smith SM, Groote IR, Westlye LT (2016) The brain functional connectome is robustly altered by lack of sleep. Neuroimage 127:324–332.

Konadhode RR, Pelluru D, Blanco-Centurion C, Zayachkivsky A, Liu M, Uhde T, Glen WB Jr, van den Pol AN, Mulholland PJ, Shiromani PJ (2013) Optogenetic stimulation of MCH neurons increases sleep. J Neurosci 33:10257–10263.

Kong D, Vong L, Parton LE, Ye C, Tong Q, Hu X, Choi B, Brüning JC, Lowell BB (2010) Glucose stimulation of hypothalamic MCH neurons involves K(ATP) channels, is modulated by UCP2, and regulates peripheral glucose homeostasis. Cell Metab 12:545–552.

Lee MG, Hassani OK, Jones BE (2005) Discharge of identified orexin/hypocretin neurons across the sleep-waking cycle. J Neurosci 25:6716–6720.

Lever C, Burton S, O'Keefe J (2006) Rearing on hind legs, environmental novelty, and the hippocampal formation. Rev Neurosci 17:111–133.

Mileykovskiy BY, Kiyashchenko LI, Siegel JM (2005) Behavioral correlates of activity in identified hypocretin/orexin neurons. Neuron 46:787–798.

Modirrousta M, Mainville L, Jones BE (2005) Orexin and MCH neurons express c-fos differently after sleep deprivation vs. recovery and bear different adrenergic receptors. Eur J Neurosci 21:2807–2816.

Nahon JL, Presse F, Bittencourt JC, Sawchenko PE, Vale W (1989) The rat melanin-concentrating hormone messenger ribonucleic acid encodes multiple putative neuropeptides coexpressed in the dorsolateral hypothalamus. Endocrinology 125:2056–2065.

Neher E, Sakaba T (2008) Multiple roles of calcium ions in the regulation of neurotransmitter release. Neuron 59:861–872.

Nir Y, Tononi G (2010) Dreaming and the brain: from phenomenology to neurophysiology. Trends Cogn Sci 14:88–100.

Pachoud B, Adamantidis A, Ravassard P, Luppi PH, Grisar T, Lakaye B, Salin PA (2010) Major impairments of glutamatergic transmission and long-term synaptic plasticity in the hippocampus of mice lacking the melanin-concentrating hormone receptor-1. J Neurophysiol 104:1417–1425.

Peyron C, Tighe DK, van den Pol AN, de Lecea L, Heller HC, Sutcliffe JG, Kilduff TS (1998) Neurons containing hypocretin (orexin) project to multiple neuronal systems. J Neurosci 18:9996–10015.

Picchioni D, Duyn JH, Horovitz SG (2013) Sleep and the functional connectome. Neuroimage 80:387–396.

Shein-Idelson M, Ondracek JM, Liaw HP, Reiter S, Laurent G (2016) Slow waves, sharp waves, ripples, and REM in sleeping dragons. Science 352: 590–595.

Sherin JE, Shiromani PJ, McCarley RW, Saper CB (1996) Activation of ventrolateral preoptic neurons during sleep. Science 271:216–219.

Shiromani PJ, Peever JH (2017) New neuroscience tools that are identifying the sleep–wake circuit. Sleep 40:zsx032.

Shiromani PJ, Kilduff TS, Bloom FE, McCarley RW (1992) Cholinergically induced REM sleep triggers fos-like immunoreactivity in dorsolateral pontine regions associated with REM sleep. Brain Res 580:351–357.

Tian L, Hires SA, Mao T, Huber D, Chiappe ME, Chalasani SH, Petreanu L, Akerboom J, McKinney SA, Schreiter ER, Bargmann CI, Jayaraman V, Svoboda K, Looger LL (2009) Imaging neural activity in worms, flies and mice with improved GCaMP calcium indicators. Nat Methods 6:875–881.

Tsunematsu T, Ueno T, Tabuchi S, Inutsuka A, Tanaka KF, Hasuwa H, Kilduff TS, Terao A, Yamanaka A (2014) Optogenetic manipulation of activity and temporally controlled cell-specific ablation reveal a role for MCH neurons in sleep/wake regulation. J Neurosci 34:6896–6909.

Verret L, Goutagny R, Fort P, Cagnon L, Salvert D, Léger L, Boissard R, Salin P, Peyron C, Luppi PH (2003) A role of melanin-concentrating hormone producing neurons in the central regulation of paradoxical sleep. BMC Neurosci 4:19.

Weber F, Chung S, Beier KT, Xu M, Luo L, Dan Y (2015) Control of REM sleep by ventral medulla GABAergic neurons. Nature 526:435–438.

Weber F, Hoang Do JP, Chung S, Beier KT, Bikov M, Saffari Doost M, Dan Y (2018) Regulation of REM and non-REM sleep by periaqueductal GABAergic neurons. Nat Commun 9:354.

Wu MF, John J, Boehmer LN, Yau D, Nguyen GB, Siegel JM (2004) Activity of dorsal raphe cells across the sleep-waking cycle and during cataplexy in narcoleptic dogs. J Physiol 554:202–215.